International Journal of Solids and Structures 50 (2013) 3674–3684

Contents lists available at ScienceDirect

International Journal of Solids and Structures

journal homepage: www.elsevier.com/locate/ijsolstr

A physical perspective of the length scales in gradient elasticity through the prism of wave dispersion

Egor V. Dontsov, Roman D. Tokmashev, Bojan B. Guzina *

Department of Civil Engineering, University of Minnesota, Minneapolis, MN 55455, United States

ARTICLE INFO

Article history:
Received 12 March 2013
Received in revised form 24 June 2013
Available online 26 July 2013

Keywords:
Gradient elasticity
Length scales
Wave dispersion

ABSTRACT

The goal of this study is to understand the physical meaning and evaluate the intrinsic length scale parameters, featured in the theories of gradient elasticity, by deploying the analytical treatment and experimental measurements of the dispersion of elastic waves. The developments are focused on examining the propagation of longitudinal waves in an aluminum rod with periodically varying cross-section. First, the analytical solution for the dispersion relationship, based on the periodic cell analysis of a bi-layered laminate and Bloch theorem, is compared to two competing models of gradient elasticity. It is shown that the customary gradient elastic model with two length-scale parameters is able to capture the dispersion accurately up to the beginning of the first band gap. On the other hand, the gradient elastic model with an additional length scale (affiliated with the fourth-order time derivative in the field equation) is shown to capture not only the first dispersion branch before the band gap, but also the band gap itself and the preponderance of the second branch. Closed form relations between the microstructure parameters and the intrinsic length scales are obtained for both gradient elasticity models. By way of the asymptotic treatment in the limit of a weak contrast between the laminae, a clear physical meaning and scaling of the length-scale parameters was established in terms of: (i) the microstructure (given by the size of the unit cell and the contrast between the laminae), and (ii) thus induced dispersion relationship (characterized by the location and the width of the band gap). The analysis is verified through an experimental observation of wave dispersion, and wave attenuation within the band gap. A comparison between the analytical treatment, the gradient elastic model with three intrinsic length scales, and experimental measurements demonstrates a good agreement over the range of frequencies considered.

1. Introduction

It is well known that the classical approaches in continuum mechanics have limitations in mimicking the behavior of materials with microstructure. For instance, the conventional theory of linear elasticity cannot capture the dispersion characteristics of body waves propagating through a material that appears to be homogeneous at the meso scale. This and other limitations provide a motivation towards developing enriched continuum models that are able to capture the size effects by introducing intrinsic length scales synthesizing the key features of the sub-scale material structure. In the context of linear elasticity, the so-called gradient elasticity models have been considered for almost half a century. A brief survey of the theory of gradient elasticity and its applications are outlined in the sequel; for a comprehensive overview of the available formulations, in terms of both static and dynamic problems, the reader is referred to Askes and Aifantis (2011).

The general theory of gradient elasticity was established in the 1960s by Toupin (1962, 1964) and Mindlin (1964). However, the problem with applying the general theory resides in a large number of intrinsic parameters, which makes the experimental measurements thereof extremely difficult. For this reason, a multitude of reduced models with a manageable number of length-scale parameters have been proposed. For instance, static theories of gradient elasticity with a single length-scale parameter are typically used to deal with the stress singularities near the crack tip (Aifantis, 1992; Gourgiotis and Georgiadis, 2009). Similar approaches aiming to mitigate the singularity at the dislocation core can be found for example in Gutkin and Aifantis (1999). Another area where the models of gradient elasticity are found to be useful is the prediction of the wave dispersion characteristics in heterogeneous or discrete systems, see e.g. (Mindlin, 1964; Muhlhaus and Oka, 1996; Gonella et al., 2011). A variety of dynamic models, that account for higher-order inertial terms and thus allow for a more detailed description of the wave dispersion, have been considered in Metrikine and Askes (2002), Askes and Metrikine (2002) and Askes and Aifantis (2009). An in-depth discussion of the dispersion phenomena brought about by the models of gradient elasticity can

* Corresponding author. Tel.: +1 612 626 0789; fax: +1 612 626 7750.
E-mail addresses: guzina@wave.ce.umn.edu, bojan7@gmail.com (B.B. Guzina).

0020-7683/$ - see front matter © 2013 Elsevier Ltd. All rights reserved.
http://dx.doi.org/10.1016/j.ijsolstr.2013.07.012

be found in Papargyri-Beskou et al. (2009) and Fafalis et al. (2012). Many such models, however, are found to be non-causal in the context of wave propagation; to deal with the causality issue, one option is to include the fourth-order time derivative (and affiliated length-scale parameter) in the formulation (Metrikine, 2006). As shown in Pichugin et al. (2008), such consideration of the fourth-order time derivative also caters for an elevated asymptotic accuracy of the models of gradient elasticity within the framework of discrete models. A detailed comparison between the dispersive characteristics of various simplified models of gradient elasticity can be found in Askes et al. (2008).

One of the biggest challenges in dealing with the theories of gradient elasticity is a physical interpretation of the featured length-scale parameters in terms of given microstructure (Askes and Aifantis, 2011). When tackling the materials with randomly distributed heterogeneities, a numerical homogenization over the representative volume element (RVE) is typically utilized (Kouznetsova et al., 2002; Kouznetsova et al., 2004; Gitman et al., 2007). In this situation, the parameters of gradient elasticity are related to the size of the RVE, although such computational platform brings little to no physical clarity when dealing with multiple length scales. Another possibility is to derive the latter from the expansion of a discrete model (Metrikine and Askes, 2002; Metrikine, 2006), described as a specific arrangement of masses and springs. One drawback of this approach, however, is the lack of a precise relationship between the discrete model and the structure of a given heterogeneous continuum. As an alternative to the foregoing treatments, one-dimensional multi-scale homogenization of a bi-layered laminate was considered in Chen and Fish (2001) and Fish et al. (2002). Such approach allows one to obtain a closed-form expression for the intrinsic length scale in terms of the parameters of the laminate. In the present investigation, it is shown that the homogenization strategy in Chen and Fish (2001) and Fish et al. (2002) amounts to a Taylor series expansion of the affiliated dispersion relationship, enabling the gradient elasticity model to capture the initial slope and the initial curvature thereof. In this case, however, the theory of gradient elasticity fails to capture the salient "meso"-frequency features brought about by the microstructure, such as the presence of the band gaps.

An experimental measurement of the length-scale parameters of gradient elasticity is likewise an arduous task, as their effect on the sensory data may be limited. For example, static methods were deployed in Aifantis (1999), Lam et al. (2003) and Askes et al. (2012), where the size effects in torsion, bending and fracture were used to determine the relevant length-scale parameters. In the context of fracture mechanics, the intrinsic length scale may be calibrated assuming the equality between the maximum principal stress and the uniaxial tensile strength of a material (Askes et al., 2012). On the other hand, the dynamic methods geared toward exposing the intrinsic length scales typically entail measurements of wave dispersion. For instance, the ultrasound wave dispersion in polycrystalline metals was studied in Savin et al. (1970), while Jakata and Every (2008) deployed neutron scattering to obtain the dispersion characteristics of cubic crystals. In Wang and Hu (2005), on the other hand, the dispersion of flexural waves in carbon nanotubes (obtained via molecular dynamic simulations) was compared to that stemming from the theories of gradient elasticity. In most wave-based techniques, however, the attention is focused on the low-frequency approximation of the germane dispersion relationship, whereby the dispersion is treated as a small correction to the "baseline" non-dispersive wave model. Unfortunately, such paradigm does not cater for distinguishing between multiple length scales of gradient elasticity, e.g. between the "static" length scales and those that are inertia-related.

To help bridge the gap, this work employs both theoretical analysis and experimental observations to shed light on the fundamental relationship between the material microstructure, wave dispersion, and equivalent-homogeneous parameters of gradient elasticity. The primary goals are to understand the physical meaning of the length-scale parameters featured by two prominent models of gradient elasticity and to attempt their measurement in an experimental setting. To facilitate the analytical treatment of the dispersion analysis, a one-dimensional problem of longitudinal wave propagation in an elastic rod with periodically varying cross-section is adopted as a modeling platform.

2. Problem statement

Consider the propagation of longitudinal waves in a non-uniform rod characterized by the periodic pattern of rectangular cuts as shown in Fig. 1. The cuts, also referred to as the "damage", endow the wave propagation problem with a length scale L (the length of the unit cell) and a dimensionless parameter $\gamma = A_2/A_1$, which describes the ratio between the damaged and intact cross-sectional areas. The analysis of the wave dispersion in such periodic system is performed from both theoretical and experimental perspectives, with the aim of establishing a link between the parameters of gradient elasticity and germane material microstructure.

3. Wave dispersion in a periodic bi-layered structure

To study dispersion of elastic waves in a homogeneous rod with varying cross-section, it is useful to first consider an equivalent one-dimensional (1D) model that assumes constant cross-section but varying material properties as shown in the right panel of Fig. 1. Assuming time-harmonic excitation at frequency ω, the governing equation for the propagation of longitudinal waves in the latter system reads

$$\frac{\partial}{\partial x}\left(E(x)\frac{\partial u}{\partial x}\right) + \rho(x)\omega^2 u = 0, \tag{1}$$

where x is the axial coordinate; u carries the implicit time factor $e^{i\omega t}$, and $\rho(x)$ and $E(x)$ signify respectively the (varying) mass density and Young's modulus of the rod. In this setting, the analysis of wave propagation through material with periodic structure can be performed using the Bloch analysis e.g. (Brillouin, 1946), which can be formulated for the unit cell as

$$\left.\begin{bmatrix} u \\ \sigma \end{bmatrix}\right|_{x=L} = e^{-ikL}\left.\begin{bmatrix} u \\ \sigma \end{bmatrix}\right|_{x=0}, \tag{2}$$

where u and $\sigma = E\,\partial u/\partial x$ denote respectively the axial displacement and affiliated normal stress, and k is the wave number. Relationship (2) can be understood as the boundary condition for the problem of wave propagation through a bi-layered material that is governed by (1). With the aid of the transfer matrix approach, on the other hand, the solution of (1) can be written as

$$\left.\begin{bmatrix} u \\ \sigma \end{bmatrix}\right|_{x=L} = \boldsymbol{T}_2\boldsymbol{T}_1\left.\begin{bmatrix} u \\ \sigma \end{bmatrix}\right|_{x=0}, \tag{3}$$

where the matrices $\boldsymbol{T}_1$ and $\boldsymbol{T}_2$ are given respectively by

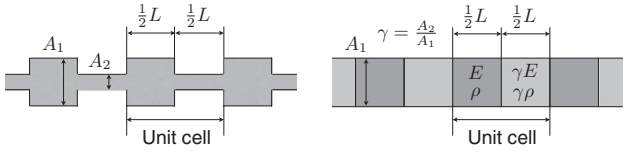

Fig. 1. Schematics of the elastic rod with rectangular cuts (left) and its 1D approximation (right).

$$\boldsymbol{T}_1 = \begin{bmatrix} \cos\left(\frac{\omega L}{2c}\right) & \frac{c}{\omega E}\sin\left(\frac{\omega L}{2c}\right) \\ -\frac{\omega E}{c}\sin\left(\frac{\omega L}{2c}\right) & \cos\left(\frac{\omega L}{2c}\right) \end{bmatrix},$$
$$\boldsymbol{T}_2 = \begin{bmatrix} \cos\left(\frac{\omega L}{2c}\right) & \frac{c}{\omega\gamma E}\sin\left(\frac{\omega L}{2c}\right) \\ -\frac{\omega\gamma E}{c}\sin\left(\frac{\omega L}{2c}\right) & \cos\left(\frac{\omega L}{2c}\right) \end{bmatrix}, \tag{4}$$

with $c = \sqrt{E/\rho}$ denoting the longitudinal wave sound speed in the rod with a constant cross section. By requiring the existence of a nontrivial solution to (2)–(4), one obtains

$$\det\left(\boldsymbol{T}_2\boldsymbol{T}_1 - e^{-ikL}\boldsymbol{I}_2\right) = 0, \tag{5}$$

where $\boldsymbol{I}_2$ is the identity matrix of size two. The solution of (5) results in the dispersion relationship

$$k = \frac{1}{L}\left[\pm\cos^{-1}\left((1+\beta)\cos\left(\frac{\omega L}{c}\right) - \beta\right) + 2n\pi\right],$$
$$\beta = \frac{1}{4}(\gamma + \gamma^{-1} - 2), \tag{6}$$

where n is an integer and β describes the contrast in material properties between two layers. Eq. (6) furnishes many families of the dispersion relationship, depending on the choice of the sign in front of the cosine function and n. In the analysis of periodic structures, the wavenumber k is typically taken from 0 to π/L, which corresponds to the first Brillouin zone e.g. (Gonella and Ruzzene, 2010), so that infinitely many frequencies correspond to each k (see the left panel in Fig. 2). This, however, may not be suitable for the problem under consideration since such dispersion relation is not reducible to $k = \omega/c$, in the case of a rod with constant cross section ($\gamma = 1$). To tackle the problem, the so called extended i.e. "unwrapped" version of dispersion relation (Brillouin, 1946) should be considered. This case, which satisfies the limiting behavior as $\gamma \to 1$, is shown in the right panel of Fig. 2 for $\beta = 0.11$. As can be seen from the display, the real part of the wave number monotonically grows with frequency while fluctuating around the straight line. Here, the observed deviation from the linear behavior diminishes for vanishing values of β and the solution converges to $k = \omega/c$ as $\beta \to 0$. One can also observe the presence of the band gaps, which feature constant real part of k and non-zero imaginary part of k. With reference to (6), the latter are bounded by the frequencies where

$$(1+\beta)\cos\left(\frac{\omega L}{c}\right) - \beta = -1 \;\Rightarrow\; \frac{\omega L}{c} = \pm\cos^{-1}\left(\frac{\beta-1}{\beta+1}\right) + 2n\pi,$$
$$n = 0, 1, 2\ldots. \tag{7}$$

In what follows, the featured (unwrapped) dispersion relationship is compared to two representative models of gradient elasticity.

4. Gradient elasticity as a low-frequency approximation

The characterization of a dispersion relationship for a material with "microstructure" such as that in Fig. 1 can also be effected within the framework of gradient elasticity (GE) (Mindlin, 1964; Askes and Aifantis, 2011). In what follows, an attempt is made to do so by making reference to two prototypical models that have been previously considered in a number of studies, see e.g. (Askes et al., 2008).

4.1. Two length-scale model

Out of a wide variety of available GE models, perhaps the most prevalent governing equation describing the (dispersive) one-dimensional wave propagation reads

$$\left(1 - h^2\frac{\partial^2}{\partial x^2}\right)\frac{\partial^2 u}{\partial t^2} = c_o^2\left(1 - l^2\frac{\partial^2}{\partial x^2}\right)\frac{\partial^2 u}{\partial x^2}, \tag{8}$$

see Mindlin (1964), where h and l are the length-scale parameters of the gradient elastic model, c_o is the zero-frequency limit of the phase velocity, and u denotes the axial displacement. On taking $u \propto e^{i(\omega t - kx)}$, one finds the dispersion relationship affiliated with (8) to read

$$k = \sqrt{\frac{-(1 - h^2\omega^2/c_o^2) \pm \sqrt{\left(1 - h^2\omega^2/c_o^2\right)^2 + 4l^2\omega^2/c_o^2}}{2l^2}}. \tag{9}$$

Here the sign in front of the inner square root should be chosen to ensure the solution with either zero or positive attenuation coefficient as will be examined later. The gradient elastic model (8) has three independent parameters, c_o, h, and l, which can be selected based on different considerations. For instance, (9) can be viewed as a low-frequency approximation of the dispersion relationship (6). With such objective, parameters c_o, h, and l are selected so that (6) and (9) have (i) the same initial slopes, and (ii) the same onset of the first band gap. These requirements produce the system of equations

$$c_o = \frac{c}{\sqrt{1+\beta}},$$
$$\frac{-(1 - h^2\omega_1^2/c_o^2)}{2l^2} = k_1^2, \tag{10}$$
$$\left(1 - \frac{h^2\omega_1^2}{c_o^2}\right)^2 + \frac{4\omega_1^2 l^2}{c_o^2} = 0,$$

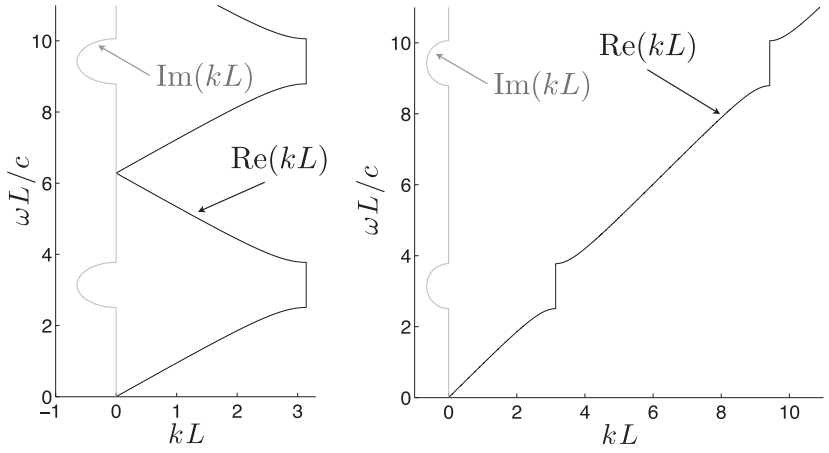

Fig. 2. Alternative representations of the dispersion relationship (6): wrapped (left) and unwrapped (right).

where

$$k_1 = \frac{\pi}{L}, \quad \omega_1 = \frac{c}{L}\cos^{-1}\left(\frac{\beta-1}{\beta+1}\right), \tag{11}$$

describe the position of the first band gap according to (7). The system of Eq. (10) can be solved to find the length-scale parameters l and h as

$$l^2 = -(1+\beta)\frac{L^2}{\pi^4}\left(\cos^{-1}\left(\frac{\beta-1}{\beta+1}\right)\right)^2,$$
$$h^2 = \frac{L^2}{1+\beta}\left(\cos^{-1}\left(\frac{\beta-1}{\beta+1}\right)\right)^{-2} - \frac{2L^2}{\pi^2}. \tag{12}$$

Note that according to (12) coefficients l^2 and h^2 may take negative values, which contradicts the notion of positive definiteness of the strain energy density in gradient-elastic solids (Mindlin, 1964). However, it is known (e.g. Mindlin, 1972) that the only way to match the wave dispersion in a lattice is to forgo the latter restriction of positive definiteness, see also Fish et al. (2002) for a particular 1D example. In this setting, the results presented herein are consistent with the observations in Mindlin (1972), as the negative values of the featured length-scale parameters are required to match the observed wave dispersion in a "damaged" rod. Furthermore, models of type (8) are typically derived as a *low-frequency* approximation (Mindlin, 1964) of a material with microstructure. Accordingly their lack of positive definiteness (when e.g. l^2 and h^2 are negative) should be interpreted in the context of this limitation. As an illustration, Fig. 3 plots a comparison between the 1D model (6) and the GE model (9) with c_o, h, and l given by (10a) and (12). In this particular case, (9) deploys positive sign in front of the inner square root both for $\omega < \omega_1$ and $\omega > \omega_1$. In general, the sign is chosen so that $\mathrm{Im}(k) = 0$ outside of the band gap, and $\mathrm{Im}(k) < 0$ within the band gap which ensures positive energy dissipation. As can be seen from the display, the first branch of the dispersion relationship (before the band gap) is well approximated by the GE model; however, the band gap itself and the second branch are poorly described by (9).

4.2. Three length-scale model

In order to describe the first band gap predicted by (6), one has to endow the gradient elasticity model with at least one additional parameter. One possibility is to include the fourth-order time derivative in the governing Eq. (8) as examined e.g. in Metrikine (2006), Pichugin et al. (2008) and Askes et al. (2008). In this case, the dispersive propagation of elastic waves is described by

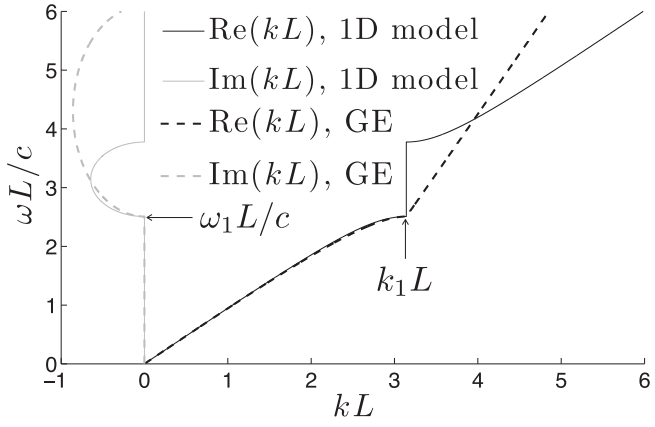

Fig. 3. Comparison in terms of the dispersion relationship between the periodic 1D model (6) with $\beta = 0.11$ and gradient elasticity model (9) with the GE parameters given by (10a) and (12).

$$\left(1 - h^2\frac{\partial^2}{\partial x^2} + \frac{s^2}{c_o^2}\frac{\partial^2}{\partial t^2}\right)\frac{\partial^2 u}{\partial t^2} = c_o^2\left(1 - l^2\frac{\partial^2}{\partial x^2}\right)\frac{\partial^2 u}{\partial x^2}, \tag{13}$$

where s is the additional length-scale parameter. The dispersion relation that corresponds to (13) reads

$$k = \sqrt{\frac{-(1 - h^2\omega^2/c_o^2) \pm \sqrt{(1 - h^2\omega^2/c_o^2)^2 + 4l^2\omega^2/c_o^2(1 - s^2\omega^2/c_o^2)}}{2l^2}}. \tag{14}$$

Again, the sign in front of the inner square root is chosen so that k is real-valued outside of the band gap, and has negative imaginary part therein. The dispersion relation (14) now involves four independent parameters, which allows the GE model to reproduce *the end* of the first band gap in terms of ω_2 in addition to the previous requirements. The system of equations, analogous to (10), can be written as

$$c_o = \frac{c}{\sqrt{1+\beta}},$$
$$\frac{-(1 - h^2\omega_1^2/c_o^2)}{2l^2} = k_1^2,$$
$$\left(1 - \frac{h^2\omega_1^2}{c_o^2}\right)^2 + \frac{4l^2\omega_1^2}{c_o^2}\left(1 - \frac{s^2\omega_1^2}{c_o^2}\right) = 0, \tag{15}$$
$$\left(1 - \frac{h^2\omega_2^2}{c_o^2}\right)^2 + \frac{4l^2\omega_2^2}{c_o^2}\left(1 - \frac{s^2\omega_2^2}{c_o^2}\right) = 0,$$

where

$$k_1 = \frac{\pi}{L}, \quad \omega_1 = \frac{c}{L}\cos^{-1}\left(\frac{\beta-1}{\beta+1}\right),$$
$$\omega_2 = \frac{c}{L}\left(2\pi - \cos^{-1}\left(\frac{\beta-1}{\beta+1}\right)\right), \tag{16}$$

are the parameters associated with the first band gap. By solving (15) and (16), one can express the GE parameters in terms of the quantities of the 1D model as

$$l^2 = -\frac{1 - (\omega_1/\omega_2)^2}{4(\pi^2 - L^2\omega_1^2/c_o^2)}L^2, \quad h^2 = \frac{c_o^2}{\omega_1^2}\left(1 + \frac{2\pi^2 l^2}{L^2}\right),$$
$$s^2 = \frac{c_o^2}{\omega_1^2}\left(1 + \frac{\pi^4 c_o^2 l^2}{L^4\omega_1^2}\right). \tag{17}$$

As an illustration, Fig. 4 shows a comparison between the dispersion relation (6) and its gradient elastic approximation given by (14), (15a) and (17). A comparison demonstrates that the modified GE model (13) with four parameters performs significantly better than its three-parameter analog (8). The dispersion behavior is now captured fairly accurately up to the end of the first band gap and further into the second branch.

4.3. Comment on the homogenization approach

A similar problem of wave dispersion through a bi-layered laminate was analyzed in Chen and Fish (2001) and Fish et al. (2002) via the homogenization procedure. By interpreting the results in Fish et al. (2002) in terms of the current notation, one finds that

$$c_o = \frac{c}{\sqrt{1+\beta}}, \quad l^2 = -\frac{\beta}{12(1+\beta)}L^2, \tag{18}$$

while the remaining GE parameters (h and s) are identically zero since the gradient elastic model used in Fish et al. (2002) has only one length scale. A comparison between (15a) and (17) on the one hand and (18) on the other reveals that the zero-frequency limit

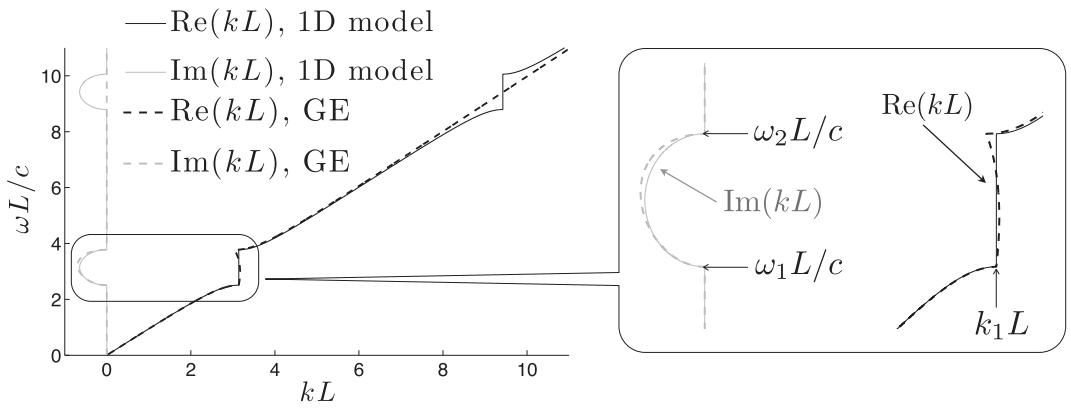

Fig. 4. Comparison in terms of the dispersion relationship between the periodic 1D model (6) with $\beta = 0.11$ and gradient elasticity model (14) with the GE parameters given by (10a) and (17).

of the phase velocity, c_o, has the same value in both treatments, while the respective formulas for the length-scale parameter l differ. To better understand the meaning of (18), one can expand (6) in Taylor series to obtain

$$\omega^2 = \frac{k^2c^2}{1+\beta}\left(1 - \frac{\beta}{12(1+\beta)}L^2k^2 + O(L^4k^4)\right). \tag{19}$$

With reference to (18), expansion (19) shows that the homogenization procedure in Fish et al. (2002) allows one to capture the initial slope and the curvature of the dispersion relationship exactly, which provides only a low-frequency approximation of the dispersion behavior (6). In contrast, the four-parameter GE model (13) with parameters given by (15a) and (17) has the ability to capture the dispersion of elastic waves through a bi-layered laminate up to, through, and past the first band gap.

4.4. Comment on the second gradient theories

For completeness, one should mention that higher-order GE models have also been proposed in the literature, such as the second gradient model in Mindlin (1965). To transcend the limitations of the latter formulation that has its roots in elastostatics, a dynamic extension of this theory was proposed in Fafalis et al. (2012), where an ad hoc assumption about the equivalence between the kinetic energies of the first-order GE model Mindlin (1964) and its second-order counterpart Mindlin (1965) has been made. By following the derivation in Fafalis et al. (2012), a one-dimensional version of the elastodynamic second gradient model can be written as

$$\left(1 - h^2\frac{\partial^2}{\partial x^2}\right)\frac{\partial^2 u}{\partial t^2} = c_o^2\left(1 - l_1^2\frac{\partial^2}{\partial x^2}\right)\left(1 - l_2^2\frac{\partial^2}{\partial x^2}\right)\frac{\partial^2 u}{\partial x^2}, \tag{20}$$

which, on taking $u \propto e^{i(\omega t - kx)}$, reads

$$\left(1 + h^2k^2\right)\omega^2 = c_o^2\left(1 + l_1^2k^2\right)\left(1 + l_2^2k^2\right)k^2. \tag{21}$$

The latter equation can be solved analytically for k to compute the germane dispersion formula. A preliminary analysis indicates that the dispersion relationship stemming from (21) is similar to (14) in that it features three parameters that can be adjusted to capture the onset (in terms of both frequency and wave number) and the width of the first band gap. However, the complexity of the problem affiliated with (21) precludes similar analytical treatment (i.e. the length-scale parameters cannot be explicitly expressed in terms of the microstructural features), which may cloud a physical interpretation of the GE parameters that is the focus of this study. For this reason, the three-parameter model (20) is not investigated in further detail.

4.5. Physical meaning of the parameters of gradient elasticity

To help understand the meaning of the (squared) length-scale parameters l^2, h^2 and s^2, it is instructive to consider the case of small contrast between the two layers comprising the unit cell, namely $\beta = \frac{1}{4}(\gamma + \gamma^{-1} - 2) \ll 1$ (see Fig. 1). In this case, expressions (17) can be expanded to the leading order in Taylor series to obtain

$$\begin{aligned} l^2 &= -\frac{L^2}{2\pi^2} + O(\sqrt{\beta}L^2), \\ h^2 &= \frac{L^2}{\pi^2}\left(\frac{3}{\pi} - \frac{\pi}{4}\right)\sqrt{\beta} + O(\beta L^2), \\ s^2 &= \frac{L^2}{2\pi^2} + O(\sqrt{\beta}L^2). \end{aligned} \tag{22}$$

As expected, l, h and s all scale linearly with L since there are no other length scales in the physical problem. However, the three parameters differ in magnitude when $\beta \ll 1$, which may be representative of many physical configurations. In particular, parameters l and s are both $O(L)$ for small β and do not vanish in the limit of a non-dispersive material ($\beta \to 0$). In this case, the key role of l and s is to reflect *the size of the unit cell*, which is primarily responsible for *the position* (frequency- and wave number-wise) *of the band gap*. In particular, from (16) and (22) it follows that the wave-number location of the first band gap, k_{bg}, is given by

$$k_{bg} \simeq \frac{1}{\sqrt{-2l^2}} \simeq \frac{1}{\sqrt{2s^2}}, \quad \beta \ll 1. \tag{23}$$

Consequently, the characteristic i.e. "center" frequency of the band gap is approximated by $\omega_{bg} = c_o k_{bg}$. In contrast the third length scale, h, is primarily responsible for *the width of the band gap*. To establish the latter claim, one may expand ω_1 and ω_2 in (16) in Taylor series and deploy the second of (22) to show that

$$\begin{aligned} \Delta\omega_{bg} &\simeq \frac{4c}{L}\sqrt{\beta} \simeq 4\pi^2\left(\frac{3}{\pi} - \frac{\pi}{4}\right)^{-1}\frac{ch^2}{L^3} \\ &= \frac{4}{\pi}\left(\frac{3}{\pi} - \frac{\pi}{4}\right)^{-1} ch^2k_{bg}^3, \quad \beta \ll 1, \end{aligned} \tag{24}$$

where the last equality makes use of the fact that $k_{bg} = \pi/L$, see (16). To illustrate the performance of the GE model (13) with approximate, physically-driven values of the length-scale parameters l, h and s, Fig. 5 shows a comparison between the dispersion relationship for the 1D bi-layered model (6) and the gradient

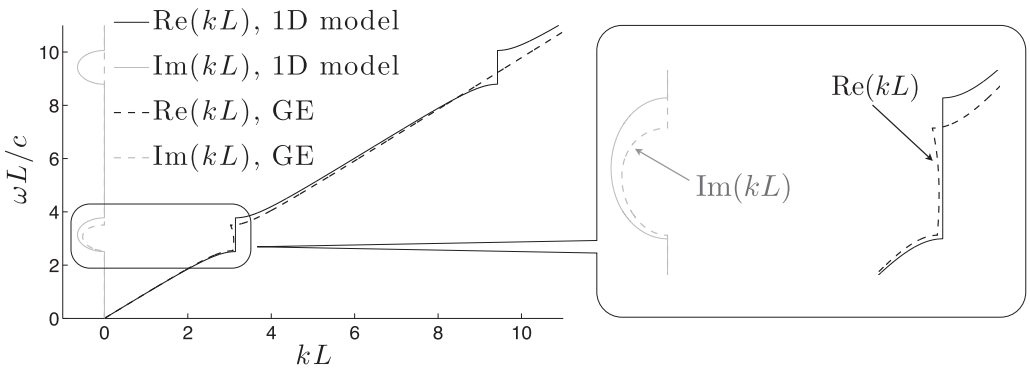

Fig. 5. Comparison in terms of the dispersion relationship between the periodic 1D model (6) with $\beta = 0.11$ and gradient elasticity model (14) with the asymptotic values ($\beta \to 0$) of the GE parameters given by (10a) and (25).

elasticity model (14) with (i) $c_o = c/\sqrt{1+\beta}$ taken to match the initial slope of the observed dispersion relationship, and (ii) the length-scale parameters taken as

$$l^2 = \frac{-1}{2k_{bg}^2}, \quad h^2 = \left(\frac{3}{\pi} - \frac{\pi}{4}\right)\frac{\pi\,\Delta\omega_{bg}}{4c\,k_{bg}^3}, \quad s^2 = \frac{1}{2k_{bg}^2}. \tag{25}$$

Fig. 5 shows that the gradient elastic model with a set of approximate parameters (25) is still able to describe the essence of the dispersion relationship in the bi-layered material. The primary advantage of (25) over (17) lies in the transparency of the physical meaning of the parameters l, h and s, which allows for a better understanding of the relation between the salient features of the dispersion relationship and corresponding gradient elastic model.

In support of the relevance of the asymptotic expressions (22) and (25), one may recall with reference to 6 and Fig. 1 that

$$\gamma := \frac{A_2}{A_1} = 1 + 2\beta - 2\sqrt{\beta^2+\beta} < 1, \tag{26}$$

which demonstrates for instance that setting $\beta < 0.1$ requires the ratio of the cross-sectional areas in Fig. 1 to be bounded as $0.54 < \gamma < 1$. In other words, the "small contrast" asymptotics 22 and 25 remain relevant even in situations where the damaged segment of the unit cell is affiliated with the 46% reduction in the cross-sectional area.

4.6. General case of an arbitrary notch length

This section considers the dispersion of elastic waves through a bi-layered structure (see Fig. 1) in a more general case when the lengths of the "narrow" and "wide" parts of the rod are different. By using symbol L to denote the overall length of the unit cell, the length of the wide part is now taken as δL ($0 < \delta < 1$), while the length of the narrow part consequently equals $(1-\delta)L$. By performing the analysis similar to that in Section 3, the dispersion relationship for such generalized bi-material rod can be derived as

$$k = \pm L^{-1}\cos^{-1}\left((1+\beta)\cos\left(\frac{\omega L}{c}\right) - \beta\cos\left(\frac{\omega(1-2\delta)L}{c}\right)\right) + \frac{2\pi n}{L},$$
$$\beta = \frac{1}{4}\left(\gamma + \gamma^{-1} - 2\right). \tag{27}$$

Unfortunately, the closed-form computation of the position k_1 of the first band gap from (27) is not possible, which precludes the analytical treatment commensurate to that in Sections 4.1 and 4.2. Alternatively, one can find ω_1 and ω_2 numerically from (27), and then use 15(a), 16(a) and 17 to find the effective values of the length-scale parameters (l, h and s) of gradient elasticity. The result is presented in Fig. 6, where the values of the normalized length-scale parameters are plotted versus δ and β. As can be seen from the display, all figures are symmetric with respect to the line $\delta = \frac{1}{2}$, which can be independently concluded from (27). Furthermore, consistent with the asymptotic expansion (22) for $\delta = \frac{1}{2}$, the variations of $|l|(\delta,\beta)$ and $s(\delta,\beta)$ are notably smaller than that of $h(\delta,\beta)$. Finally, the limit of the featured distributions as $\beta \to 0$ is also consistent with (22) since $1/(\sqrt{2}\pi) \approx 0.225$.

5. Experimental study

To investigate the dispersion of longitudinal waves in an experimental setting, measurements were performed on aluminum rods with periodically varying rectangular cross-section. Fig. 7 shows the schematics of the experimental setup, where the cross-section of the intact portion of the rod is square and measures 1.3 cm× 1.3 cm, while the damaged section is comprised of unit cells characterized by length L and damage coefficient $\gamma = A_2/A_1 = 0.525$. Each rod was hung horizontally using supporting fishnet loops (not shown) placed evenly to reduce sagging. A compressional (P-wave) ultrasonic transducer, used to generate the axial motion,

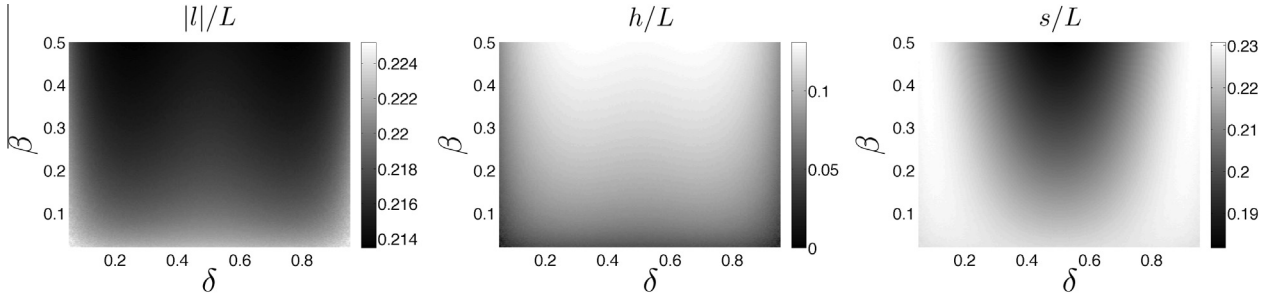

Fig. 6. Variation of the normalized parameters of gradient elasticity $|l|/L$ (left), h/L (center) and s/L (right) versus δ and β.

was glued to the left end of the rod, while the other end was glued to a stationary wall as shown in Fig. 7. To compensate for the weight of the transducer and connecting cable, an additional fish-net loop was placed near the left end of the rod. For the purpose of having a narrow-band input signal, the transducer was excited by a modulated 5-cycle sine burst with carrier frequency f_c as shown in Fig. 9. A three-dimensional Laser Doppler Vibrometer (LDV) system PSV-400 by Polytec, shown in Fig. 8, was used to capture the time histories of the axial motion at scan points. Due to imperfections in the weight distribution along the rod and misalignment of the transducer, the motion generated in the rod included both longitudinal and flexural waves. To facilitate the temporal separation between the longitudinal wave and its (slower) flexural counterpart, the first set of observation points (referred to as the "scan points before damage" in Fig. 7) were placed 60 cm away from the excitation transducer, with 5 cm separation between the neighboring points. To capture the dispersive behavior of longitudinal waves traveling through the damaged section (i.e. the section with microstructure), the second set of observation points, again with 5 cm separation, were located right after the series of two-sided rectangular grooves that were approximately 0.3 cm deep as shown in Fig. 7. A cross-correlation technique was used to determine the phase shift between the measured signals before and after the damaged section, using multiple scan points for better accuracy. This information is then used to estimate the phase velocity at a given carrier frequency f_c. In this setting, the dispersion relationship is constructed experimentally by repeating the measurements over a representative set of carrier frequencies f_c. To determine the value of the attenuation coefficient, the peak amplitudes before and after the damaged section were utilized. Note that the amplitude of the transmitted wave was also affected by the reflections from the ends of the damaged section; within the band gap (where the amplitudes matter), however, these reflections were found to reduce the transmitted wave by roughly 5% and were consequently disregarded. The three laser heads of the LDV system were positioned at an optimal distance of approximately 90 cm from the rod, which allowed for the sensing of axial motion at all scan points without readjusting. To increase the sensitivity of the non-contact motion measurements and to accurately reconstruct the axial motion in the rod, the left and right laser heads were spread apart by approximately 1 m (see Fig. 8). Each scan point was treated with a small piece of retroreflective 3M tape (see Fig. 7) to enhance the backscattering and improve the signal-to-noise characteristics of

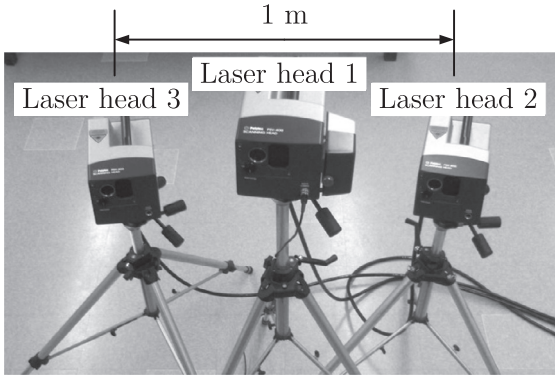

Fig. 8. The LDV system used to capture the longitudinal motion (particle velocity) in a rod.

the measured signals. The acquisition was performed using velocity decoder VD-03 with the sensitivity set to 10 mm/(s·V) and the sampling rate $F_s = 2.56$ MHz. For each scan point, signal stacking over 50 realizations was used to minimize the effect of ambient vibrations. All onboard LDV filters, both analog and digital, were turned off to avoid systematic phase errors in the measurements. Thus captured motion i.e. particle velocity signals were filtered afterwards with a simple band-pass filter over the frequency intervals $[0.2f_c, 3f_c]$ and $[0.95f_c, 1.05f_c]$, catering respectively for the measurements of the phase velocity and attenuation coefficient.

To illuminate experimentally the physical meaning of the length-scale parameters featured in the GE model, three rods were

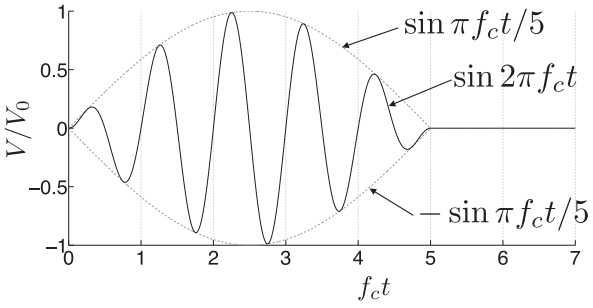

Fig. 9. Normalized voltage of the input signal versus dimensionless time.

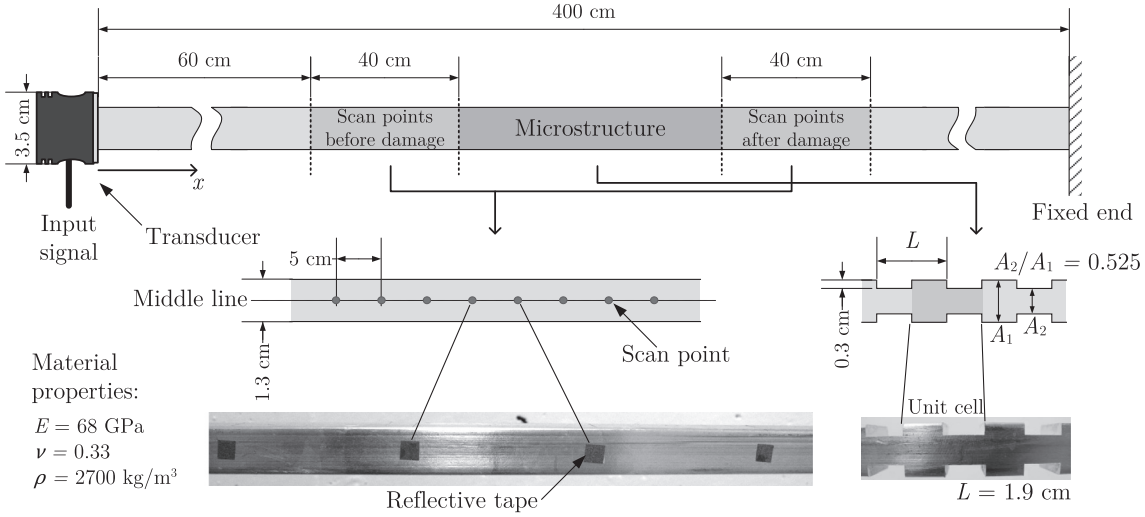

Fig. 7. Schematics of the experimental setup.

prepared with different lengths of the *unit cell* comprising the damaged section, namely $L = 1.9$ cm, $L = 6$ cm, and $L = 8$ cm (see Fig. 7). Consistent with the assumptions made in Sections 4.1 and 4.2, the lengths of the damaged and intact segments of each unit cell were made to be equal. Note that the depth of the two-sided grooves was kept *fixed*, so that the ratio $\gamma = A_2/A_1 = 0.525$ and consequently parameter $\beta = 0.108$ were common for all rods. To examine the dispersion of elastic waves through the sections with microstructure, the frequency range in terms of the carrier signal is taken as $f_c \in [10\text{ kHz},75\text{ kHz}]$ for all three specimens. At certain frequencies, however, the rods with $L = 6$ cm and $L = 8$ cm experienced severe amplitude decay affiliated with the presence of the band gap. To accurately capture the effect of attenuation, additional scan points were introduced inside the damaged section, which allowed for precise tracking of the amplitude decay. As an illustration, Fig. 10 shows the normalized peak amplitude of the axial motion (in terms of particle velocity) measured along the damaged section for $f_c \in [20\text{ kHz},40\text{ kHz}]$ in the rod with $L = 8$ cm. Here, all points corresponding to $f_c = \text{const.}$ are normalized by the peak amplitude at the first scan point, located 60 cm away from the excitation transducer. As can be seen from the display, the presence of the microstructure results in an exponential-type decay of longitudinal waves at frequencies near $f_c = 30$ kHz, which greatly reduces the motion amplitude after the damaged section. In addition, Fig. 10 features a notable increase in the amplitude near the interface between the damaged section and intact rod ($x = 140 \div 150$ cm) for input frequencies away from the band gap. This feature is related to the wave reflections that are inevitable due to impedance mismatch between the damaged section and the intact part of the rod.

Undamaged rod. In general, the longitudinal waves in a rod exhibit dispersive behavior when the dominant wavelength becomes comparable to the thickness of the rod. In this study, the magnitude of such induced dispersion is comparable or less than that due to the presence of microstructure. To effectively investigate the dispersion induced solely by the microstructure, the variation of the longitudinal wave speed versus frequency is first measured *in the intact rod* and then "subtracted" from the observed (aggregate) dispersion relationship. Fig. 11 plots the variation of the phase velocity of longitudinal waves in the intact rod versus frequency. The error bars reflect the standard deviation, computed from the measurements taken at different scan points. Here, the main source of error is a limited resolution of the distance measurements used to locate the scan points, estimated at 1 mm. Fig. 11 also shows the polynomial fit of the data, which can be written as

$$\frac{c_{\text{int}}}{c} = 1 - \left(\frac{a_1\,\omega}{c}\right)^2 - \left(\frac{a_2\,\omega}{c}\right)^4, \tag{28}$$

where c_{int} denotes the phase velocity in the intact rod; $c = \sqrt{E/\rho} = 5023$ m/s, $a_1 = 1.3$ mm, and $a_2 = 2.3$ mm. In what follows, this relation is used to nullify the dispersion due to finite cross-sectional dimensions of the rod.

Augmented 1D model. From a preliminary comparison between the experimental results and the 1D model described in Section 3, it became apparent that the simplistic one-dimensional model is suitable only for qualitative analysis. In particular, the position and the width of the band gap were captured admissibly well, while the slope of the dispersion relationship was notably overestimated – even at low frequencies. This difference shows the limitation of the 1D model, which is not capable of accurately reproducing the 2D features of the rod with notches. One straightforward solution is to solve the 2D elastodynamic problem via e.g. the finite element method and to obtain the desired dispersion relationship numerically. Another option, that is adopted in this study, mitigates the limitations of the original approximation and is able to match the experimental data without onerous departure from the one-dimensional framework. With reference to the left panel in Fig. 1, the main limitation of the original 1D model resides in the premise that the normal stress across any section of the rod is constant, including intact sections that are close to the interface with the damaged segment. To overcome this problem and account for the non-uniform sectional distribution of stress near the interfaces, it is useful to assume the variation of the mass density and Young's modulus over the length of the unit cell as shown in Fig. 12. With reference to Figs. 1 and 12, the mass density distribution accordingly remains unchanged while the Young's modulus within the intact segment of the unit cell varies as

$$E \longrightarrow \eta(x')E, \quad \eta(x') = \min\left(1, \gamma + (1-\gamma)\frac{x'}{\ell}, \gamma + (1-\gamma)\frac{\frac{1}{2}L - x'}{\ell}\right), \quad 0 < x' < \frac{1}{2}L, \tag{29}$$

where $x' = x - x_c$, x_c denotes the position of the left end of the unit cell, and the transition length ℓ is selected so that the augmented model matches the observed phase velocity of longitudinal waves (through the damaged segment) at low frequencies. For consistency, the same value of ℓ is used for all configurations regardless of the length L of the unit cell.

For completeness, one should note that the dispersion relationship for the above augmented 1D model cannot be calculated

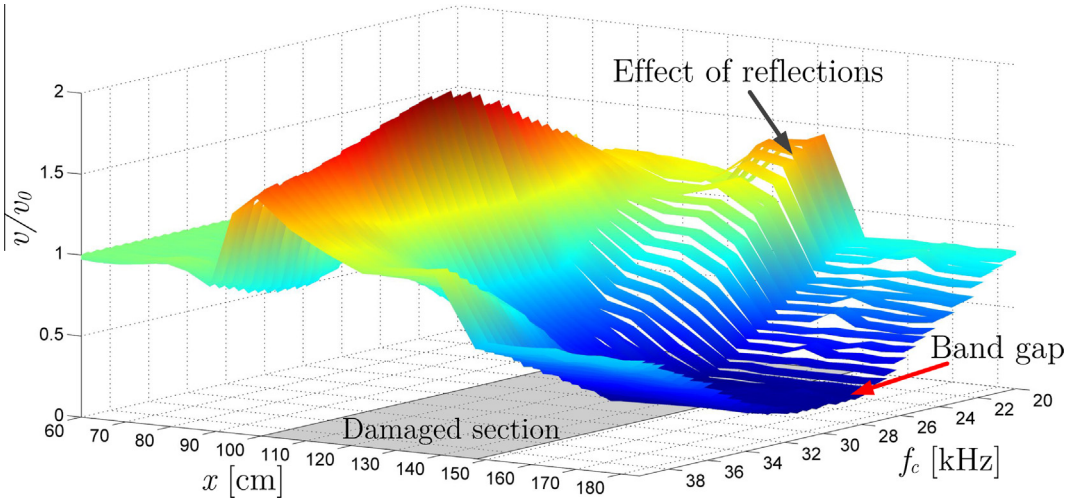

Fig. 10. Distribution of the peak particle velocity in the aluminum rod ($L = 8$ cm) for $f_c = 20 \div 40$ kHz.

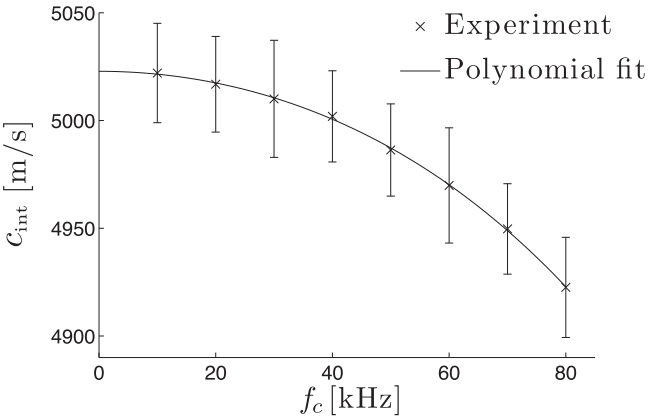

Fig. 11. Variation of the longitudinal phase velocity versus frequency for the intact rod.

analytically; instead, the numerical treatment via the transfer matrix approach (as in Section 3) is used to solve the problem and consequently compute the parameters c_o, ω_1 and ω_2 that are needed for the calibration of the GE model.

Rods with microstructure. To facilitate the interpretation of the experimental measurements, it is noted with reference to Fig. 4 that the wave number k featured in the latter diagram can be conveniently written as

$$k = \frac{\omega}{c_{\rm dam}} - \mathrm{i}\alpha,$$

where $c_{\rm dam}$ is the phase velocity of the longitudinal waves propagated through the damaged section, and $\alpha \geqslant 0$ is the attenuation coefficient characterizing the affiliated exponential decay of wave amplitude (if any). As an example, Fig. 13 plots the variation of the normalized phase velocity in the damaged segment, $c_{\rm dam}/c_{\rm int}$, versus frequency for the rod with $L = 1.9$ cm. Due to the constraints imposed by the experimental approach, the carrier frequency f_c of the input signal is assumed to take the role of the excitation frequency $\omega/(2\pi)$. Here the normalization of the observed phase velocity by $c_{\rm int}$, computed via (28), allows one to "subtract" the dispersion caused by the finite cross-sectional dimensions of the intact rod. As before, the error bars reflect the standard deviation computed from the measurements taken at different scan points. Note that the augmented 1D model (the solid line in Fig. 13) features the transition length $\ell = 8.5$ mm, found to provide the best fit with the experimental data. In general, ℓ shifts the dispersion curve of the 1D model in the vertical direction without noticeably distorting its shape. The gradient elastic model (13) with the length-scale parameters computed according to (17) is indicated by the dashed line. In this case, the parameters of gradient elasticity take values $c_o = 4375$ m/s, $|l| = 4.2$ mm, $h = 1.24$ mm, and $s = 4.2$ mm. It is worth noting that the featured length scales compare favorably with their low-contrast estimates (22) of $|l| = 4.3$ mm, $h = 1.43$ mm and $s = 4.3$ mm, despite the underpinning incompatibilities introduced by the augmented 1D model. As can be seen from the display, the overall agreement between the dispersion curves is admissible. Also note that since $2\ell = 17$ mm $> L/2 = 9.5$ mm, an overlapping of the transition zones shown in Fig. 12 takes place in which case $\eta(x') < 1$ throughout the intact zone of the unit cell, see (29). In general, the approximations introduced by the premise of one-dimensional wave propagation, including those stemming from (29), are the main cause of the discrepancies observed in Fig. 13.

Fig. 14 shows the results of the experimental measurements for the rod with $L = 6$ cm. The left panel plots the variation of the phase velocity versus the carrier frequency, while the right panel describes the corresponding variation of the attenuation

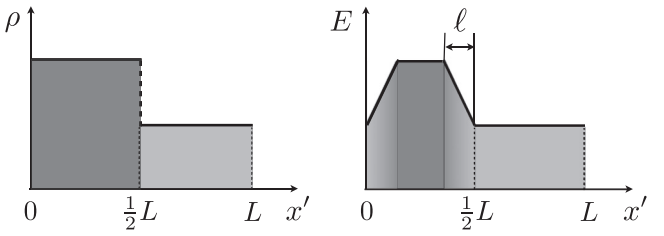

Fig. 12. Schematics of the variation of the mass density (left) and the Young's modulus (right) over the unit cell of the augmented 1D model.

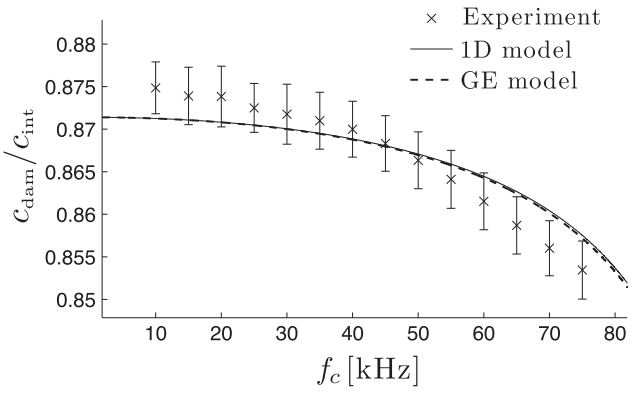

Fig. 13. Variation of the normalized phase velocity in the rod with $L = 1.9$ cm.

coefficient. The solid lines show the predictions of the augmented 1D model ($\ell = 8.5$ mm), while the dashed lines indicate the corresponding gradient elastic approximation. The calculated parameters of gradient elasticity are $c_o = 4607$ m/s, $|l| = 13.2$ mm, $h = 4.8$ mm and $s = 13$ mm. As a point of reference, it is noted that the low-frequency approximation (22) in this case yields $|l| = 13.5$ mm, $h = 4.5$ mm and $s = 13.5$ mm. Clearly, the results in Fig. 14 for $L = 6$ cm are qualitatively different from those in Fig. 13 for $L = 1.9$ cm since the former feature a band gap (shown as a shaded area) within the featured frequency range. As can be seen from the display, the band gap features non-zero attenuation coefficient and represents the transition zone between two branches of phase velocity. Note that the magnitude of the dispersion in Fig. 14 ($L = 6$ cm) is roughly an order of magnitude higher than that in Fig. 13 ($L = 1.9$ cm). Further, it is seen that the agreement between the measurements and the 1D model at low frequencies (below 25 kHz) is significantly better for $L = 6$ cm than for $L = 1.9$ cm. This can be explained by the smaller contribution of the "ℓ" correction, see (29), introduced by the augmented 1D model. One may also note that the observed values of the phase velocity in Fig. 14 seem to follow a smooth curve, which is not observed by the model. The principal reason for such disagreement resides in the multi-frequency nature of the transient pulse, whereby each measurement point along the *carrier frequency* axis represents an average between the neighboring frequencies. This "averaging" is one possible reason for the "smoothing" of experimental data. Another possible reason for the observed discrepancy is the presence of the 2D features (in terms of non-axial wave propagation) that are not captured by 1D model. Regarding the attenuation coefficient, the error bars in the right panel of Fig. 14 are computed on the basis of the ratio between the observed motion amplitude after the damaged section and the noise level. For this reason, the error bars for the attenuation coefficient are higher inside the band gap since the amplitude of the signal reduces dramatically after passing through the damaged section.

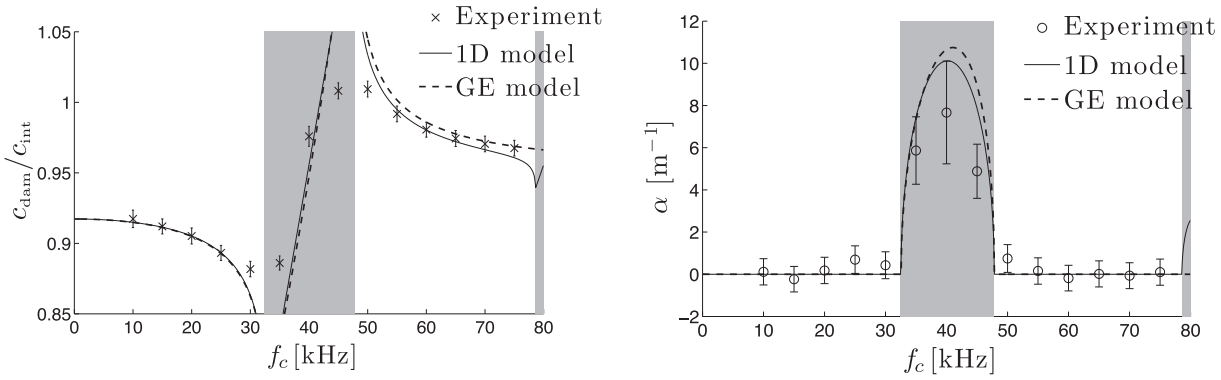

Fig. 14. Variation of the normalized phase velocity (left) and attenuation coefficient (right) in the rod with $L = 6$ cm.

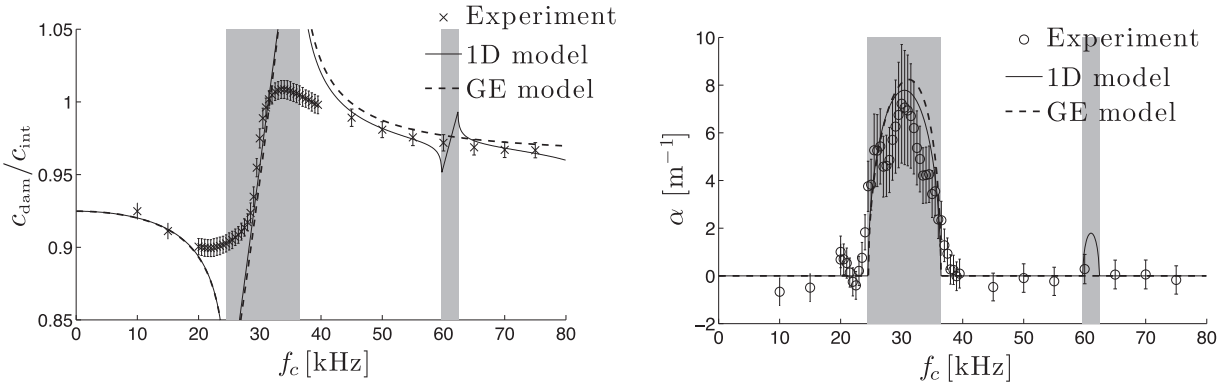

Fig. 15. Variation of the normalized phase velocity (left) and attenuation coefficient (right) in the rod with $L = 8$ cm.

The results of experiments for the rod with $L = 8$ cm are shown in Fig. 15. The left panel plots the phase velocity versus the carrier frequency, while the right panel plots the corresponding variation of the attenuation coefficient. The markers correspond to the experimental measurements, the solid lines stand for the augmented 1D model ($\ell = 8.5$ mm), and the dashed lines represent the gradient elastic model whose parameters are fitted to the 1D model. The calculated parameters of gradient elasticity are $c_o = 4645$ m/s, $|l| = 17.6$ mm, $h = 6.1$ mm and $s = 17.3$ mm, again showing consistency with the low-contrast estimates (22) of $|l| = 18$ mm, $h = 6.0$ mm and $s = 18$ mm. Note that there is almost no qualitative difference between the results in Fig. 14 and Fig. 15. Both sets of experimental results feature a band gap that is well represented by the 1D and GE models, as well the prediction of the second band gap that is not supported by the experimental data. One explanation for this disagreement is again the multi-frequency excitation source, whereby each measurement "point" in terms of f_c represents an average over the range of neighboring frequencies. With reference to Fig. 9, the width of this frequency range (over which the smearing occurs) is on the order of 10% of the carrier frequency, e.g. 6 kHz for $f_c = 60$ kHz. Since the width of the second band gap in Fig. 15 is notably smaller than 6 kHz, it is not surprising that the latter cannot be resolved via the featured experimental approach that relies on the propagation of narrow-band pulses – as opposed to true monochromatic testing.

For convenience, Table 1 summarizes the length scales of the gradient elasticity model (13) as identified from the wave dispersion experiments on the three rods with microstructure. In the chart, also included are their low-contrast asymptotic estimates ($|l|^{\rm as}, h^{\rm as}$ and $s^{\rm as}$) as computed directly from the microstructural parameters of each rod following (22). Overall, the agreement between the two sets of estimates can be qualified as remarkable,

Table 1
Length scales of the gradient elasticity model (13) for the rods tested.

L (mm)	β	$\lvert l\rvert$ (mm)	h (mm)	s (mm)	$\lvert l\rvert^{\rm as} = s^{\rm as} = \frac{L}{\sqrt{2}\pi}$ (mm)	$h^{\rm as} = \sqrt{\frac{3}{\pi} - \frac{\pi}{4}}\frac{L\beta^{1/4}}{\pi}$ (mm)
19	0.108	4.2	1.24	4.2	4.3	1.43
60	0.108	13.2	4.8	13.0	13.5	4.5
80	0.108	17.6	6.1	17.3	18.0	6.0

lending credence to the intimate relationship between the microstructure, the affiliated dispersion characteristics, and the effective length scales of gradient elasticity that is exposed through this investigation.

6. Summary

This study investigates the dispersion of longitudinal waves in a rod with periodic "microstructure" (or damage) by means of the analytical treatment, theory of gradient elasticity, and experimental measurements. First, the problem of wave propagation in a damaged rod (with a periodic pattern of rectangular notches) is approximated as that through a one-dimensional bi-layered structure. The dispersion relationship is then obtained using periodic cell analysis and Bloch theorem. Two prominent models of gradient elasticity are deployed to approximate the dispersion relation stemming from the 1D model. It is shown that the "usual" gradient elastic model with two length-scale parameters is capable of capturing the dispersion of elastic waves accurately up to the beginning of the first band gap. In contrast, the gradient elastic model with an additional length scale, responsible for the fourth-order

time derivative in the governing equation, is shown to capture not only the first dispersion branch before the band gap, but also the entirety of the band gap and a larger part of the second branch. Closed-form relationships between the parameters of the microstructure and the intrinsic length scales are obtained for both gradient elasticity models. By way of the asymptotic treatment in the limit of a small contrast between the layers, a lucid physical meaning and scaling of the length-scale parameters of gradient elasticity was established in terms of both (i) the microstructure, as given by the size of the unit cell and the contrast between laminae, and (ii) the induced dispersion relationship, as characterized by the initial slope and the features of the first band gap. The analysis is supported through the experimental observations of longitudinal wave dispersion and attenuation through a set of aluminum rods with periodic "microstructure". To mitigate the inaccuracies brought about by the simplifying assumptions of the 1D model, the so-called augmented 1D model is introduced, where the discontinuous variation of the effective Young's modulus is replaced by a continuously varying function. This enhancement allowed the 1D periodic model and its gradient elasticity counterpart to accurately capture the dispersion and attenuation data measured in the damaged aluminum rods over the frequency range from 10 kHz to 75 kHz, which includes the first band gap and the beginning of the second branch. Thus identified length scales of gradient elasticity showed a remarkable agreement with their (small-contrast) asymptotic approximations for all experimental configurations considered.

Acknowledgments

The authors are grateful to Mr. Simon Humbert who, as an undergraduate student from Ecole Polytechnique, France, spent his internship at the University of Minnesota and helped jump-start the project with two-dimensional finite element simulations of the longitudinal waves in rods with microstructure.

References

Aifantis, E., 1992. On the role of gradients in the localization of deformation and fracture. Int. J. Eng. Sci. 30, 1279–1299.
Aifantis, E., 1999. Strain gradient interpretation of size effects. Int. J. Fract. 95, 299–314.
Askes, H., Aifantis, E., 2009. Gradient elasticity and flexural wave dispersion in carbon nanotubes. Phys. Rev. B 80, 195412.
Askes, H., Aifantis, E., 2011. Gradient elasticity in statics and dynamics: An overview of formulations, length scale identification procedures, finite element implementations and new results. Int. J. Solids Struct. 48, 1962–1990.
Askes, H., Metrikine, A., 2002. One-dimensional dynamically consistent gradient elasticity models derived from a discrete microstructure: Part 2: Static and dynamic response. Eur. J. Mech. A Solids 21, 573–588.
Askes, H., Metrikine, A., Pichugin, A., Bennett, T., 2008. Four simplified gradient elasticity models for the simulation of dispersive wave propagation. Philos. Mag. 88, 3415–3443.
Askes, H., Calik-Carakose, U., Susmel, L., 2012. Gradient elasticity length scale validation using static fracture experiments of PMMA and PVC. Int. J. Fract. 176, 223–227.
Brillouin, L., 1946. Wave Propagation in Periodic Structures. Dover, New York.
Chen, W., Fish, J., 2001. A dispersive model for wave propagation in periodic heterogeneous media based on homogenization with multiple spatial and temporal scales. J. Appl. Mech. 68, 153–161.
Fafalis, D., Filopoulos, S., Tsamasphyros, G., 2012. On the capability of generalized continuum theories to capture dispersion characteristics at the atomic scale. Eur. J. Mech. A Solids 36, 25–37.
Fish, J., Chen, W., Nagai, G., 2002. Non-local dispersive model for wave propagation in heterogeneous media: one-dimensional case. Int. J. Num. Methods Eng. 54, 331–346.
Gitman, I., Askes, H., Aifantis, E., 2007. Gradient elasticity with internal length and internal inertia based on the homogenisation of a representative volume element. J. Mech. Behav. Mater. 18, 1–16.
Gonella, S., Ruzzene, M., 2010. Multicell homogenization of one-dimensional periodic structures. J. Vib. Acoust. 132, 011003.
Gonella, S., Greene, M., Liu, W., 2011. Characterization of heterogeneous solids via wave methods in computational microelasticity. J. Mech. Phys. Solids 59, 959–974.
Gourgiotis, P., Georgiadis, H., 2009. Plane-strain crack problems in microstructured solids governed by dipolar gradient elasticity. J. Mech. Phys. Solids 57, 1898–1920.
Gutkin, M., Aifantis, E., 1999. Dislocations in the theory of gradient elasticity. Scr. Mater. 40, 559–566.
Jakata, K., Every, A., 2008. Determination of the dispersive elastic constants of the cubic crystals Ge, Si, GaAs, and InSb. Phys. Rev. B 77, 174301.
Kouznetsova, V., Geers, M., Brekelmans, W., 2002. Multi-scale constitutive modelling of heterogeneous materials with a gradient-enhanced computational homogenization scheme. Int. J. Numer. Methods Eng. 54, 1235–1260.
Kouznetsova, V., Geers, M., Brekelmans, W., 2004. Size of a representative volume element in a second-order computational homogenization framework. Int. J. Multiscale Comput. Eng. 2, 575–598.
Lam, D., Yang, F., Chong, A., Wang, J., Tong, P., 2003. Experiments and theory in strain gradient elasticity. J. Mech. Phys. Solids 51, 1477–1508.
Metrikine, A., 2006. On causality of the gradient elasticity models. J. Sound Vib. 297, 727–742.
Metrikine, A., Askes, H., 2002. One-dimensional dynamically consistent gradient elasticity models derived from a discrete microstructure: Part 1: Generic formulation. Eur. J. Mech. A Solids 21, 555–572.
Mindlin, R., 1964. Microstructure in linear elasticity. Arch. Ration. Mech. Anal. 16, 51–78.
Mindlin, R., 1965. Second gradient of strain and surface-tension in linear elasticity. Int. J. Solids Struct. 1, 417–438.
Mindlin, R., 1972. Elasticity, piezoelectricity and lattice dynamics. J. Elast. 2, 217–282.
Muhlhaus, H.-B., Oka, F., 1996. Dispersion and wave propagation in discrete and continuous models for granular materials. Int. J. Solids Struct. 33, 2841–2858.
Papargyri-Beskou, S., Polyzos, D., Beskos, D., 2009. Wave dispersion in gradient elastic solids and structures: A unified treatment. Int. J. Solids Struct. 46, 3751–3759.
Pichugin, A., Askes, H., Tyas, A., 2008. Asymptotic equivalence of homogenisation procedures and fine-tuning of continuum theories. J. Sound Vib. 313, 858–874.
Savin, G., Lukashev, A., Lysko, E., 1970. Elastic wave propagation in a solid with microstructure. Int. Appl. Mech. 6, 725–728.
Toupin, R., 1962. Elastic materials with couple stresses. Arch. Ration. Mech. Anal. 11, 385–414.
Toupin, R., 1964. Theories for elasticity with couple-stress. Arch. Ration. Mech. Anal. 17, 85–112.
Wang, L., Hu, H., 2005. Flexural wave propagation in single-walled carbon nanotubes. Phys. Rev. B 71, 195412.